ROYAL SOCIETY OF CHEMISTRY

PAPER

Check for updates

Biomass-derived surface-functionalized graphene quantum dots for aggregation-induced green fluorescence

Syed Adil Shah, (ID) *[a] Eman Gul[b] and Syed Niaz Ali Shah (ID) *[c]

In the realm of nanomaterials, surface modification and vacancy defects are widely recognized as key factors that influence various physical and chemical properties. However, the creation and dynamic structural evolution of vacancy defects in atomically thin graphene quantum dots (GQDs) remain largely unexplored, primarily due to the challenges in isolating GQDs that exhibit such defects. In this study, nitrogen-doped GQDs (size *ca.* 3 nm) were synthesized from biomass extracts and subsequently surface functionalized to enhance their properties. Interestingly, the functionalization process not only introduced inner defects but also promoted the aggregation of GQDs, which, in turn, led to a significant boost of green fluorescence. The successful synthesis of GQDs and the incorporation of functional groups were confirmed using various characterization techniques. UV-vis spectroscopy was employed to identify the characteristic optical signatures of GQDs, while FTIR spectroscopy verified the presence of specific functional groups. Dark-field scanning transmission electron microscopy (STEM) was utilized for size authentication, visualization of inner defects, and insights into the morphological features of the GQDs. X-ray photoelectron spectroscopy was employed for elemental analysis. Additionally, luminescence studies, including fluorescence and photoluminescence, were conducted to investigate the optical properties. The meticulously prepared surface-functionalized GQDs, showcasing elevated luminescence, hold significant promise as advanced multifunctional materials. Their semiconducting nature makes them strong candidates for high-performance display applications, while their exceptional biocompatibility and robust fluorescence position them as an ideal platform for drug delivery, particularly in cancer therapeutics.

1. Introduction

The development of graphene quantum dots (GQDs) has gained impetus for various applications due to numerous benefits, typically long-lasting photostability, non-toxicity, cost-effectiveness, color tunability, and particularly their strong potential for biomedical applications.[1–4] GQDs belong to the category of zero-dimensional (0-D) fluorescent carbon nanomaterials, which have a lot of edge states and functional groups along with a noticeable quantum confinement effect, characterized by a lateral size smaller than 10 nm.[5,6] Functionalized-GQDs exhibit better photo-response than GQDs in optoelectronic devices because of improved carrier transport.[7–10] The presence of these functional groups imparts notable hydrophilic properties to GQDs, enhancing their optical characteristics and ensuring favorable biocompatibility and non-

toxicity.[3,11] In practical terms, GQDs have gained significant recognition for their extensive utilization in the human body environment, particularly in cell imaging applications.[2,12]

Structurally, GQDs exhibit features similar to both fullerenes and carbon dots (CDs), comprising primarily sp²-hybridized carbon atoms, with localized sp³ sites bearing oxygen-containing groups.[13–15] However, unlike CDs, which are generally dominated by sp³ hybridization and display an amorphous structure, GQDs are characterized by sp² hybridization and well-defined crystalline domains.[16–18] This fundamental structural distinction translates to differences in their electronic and optical behavior, making GQDs more attractive for applications requiring tunable luminescence and advanced electronic functionality.

To modulate the optical and electrical properties of GQDs, surface modification is often employed, with heteroatom doping, using elements like N, S, F, Cl, and B, being a widely adopted strategy.[19–21] Such doping serves as an effective structural modification technique that can enhance the ability of GQDs to scavenge free radicals. The photoluminescence (PL) behaviour of the GQDs is influenced by charge transfer between the functional groups and the QDs.[22] Furthermore, chemical

[a]School of Biomedical Engineering, Health Science Centre, Shenzhen University, Shenzhen, Guangdong 518060, PR China. E-mail: syedshahkhan2141@gmail.com
[b]Institute of Chemical Sciences, University of Peshawar, Peshawar 25000, Pakistan
[c]Innovation and Technology Transfer, King Fahd University of Petroleum and Minerals, Dhahran 31261, Saudi Arabia. E-mail: niazalianalyst@gmail.com
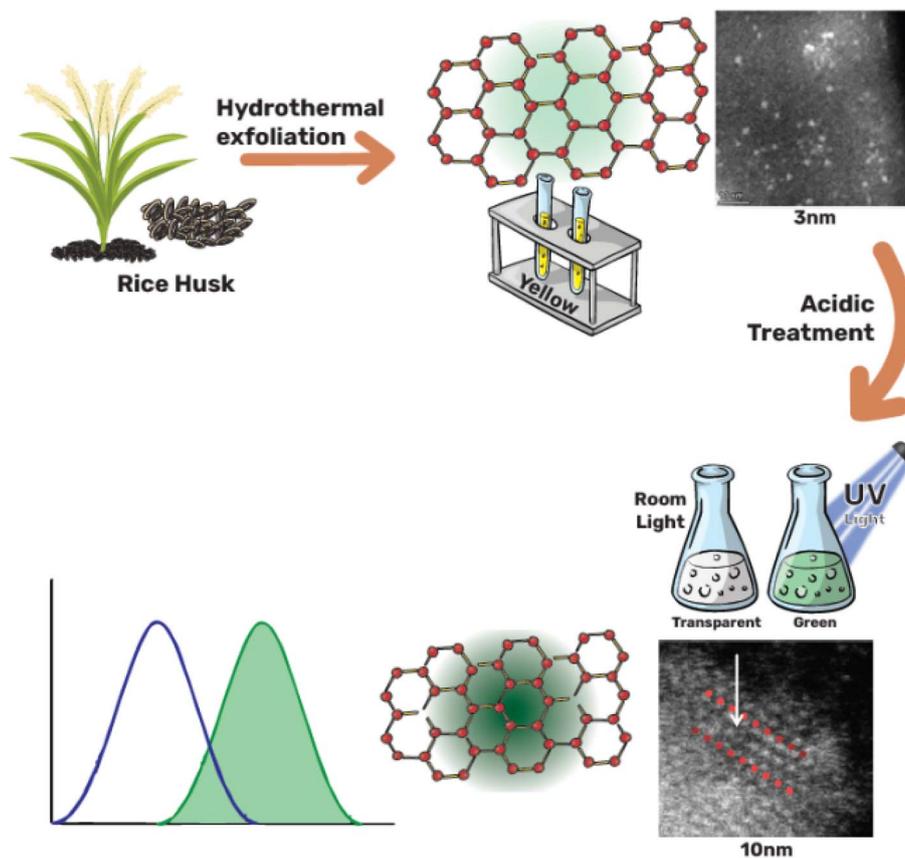
Scheme 1 Schematic illustration of the green synthesis of graphene quantum dots (GQDs), where subsequent aggregation-induced emission and defect formation contribute to enhanced fluorescence.

functionalization can alter their energy gap and total dipole moment, thereby modifying their entire characteristics.[23] Ultimately, the optical and electrical properties of GQDs depend not only on their shape, but also on the type and position of the attached functional group.[24–26] For instance, hexagonal-armchair GQDs have strong fluorescence properties.[27,28] The luminescence and bandgap of GQDs can be tuned by adjusting parameters such as the number of layers, size, shape, and edge morphology.[29] Oxygen-based edge passivation, in particular, has been shown to reduce the energy gap.[30] Functional groups containing oxygen, such as –OH, –CHO, –COCH$_3$, and –COOH, are frequently utilized to alter the electrical and optical characteristics of GQDs.[31] Groups like –OH and –COOH can induce a redshift in emission and decrease the energy gap.[32]

Heteroatom doping remains one of the most effective strategies for achieving such modifications, as dopant atoms incorporated into the GQD lattice can alter the energy band structure, polarizability, defect density, local electron configuration, and elemental composition.[33–35] These structural and electronic changes directly influence the physical and chemical characteristics of GQDs, including their catalytic activity, PL characteristics, size, and surface morphology.[36,37] Their strong PL, coupled with a high density of reactive surface groups, enables versatile conjugation with a wide range of therapeutic agents, including ligands, polymers, fluorescent dyes, light-

responsive materials, and functional nanoparticles.[38] This remarkable conjugation capability underscores graphene's significance in biomedical applications, particularly in cancer diagnostics and therapy.[39] Notably, certain heteroatom dopants can enhance fluorescence, while others may quench it, depending on their nature and interaction with the GQD structure.

However, achieving a practical green light emission from GQDs requires two critical parameters: a narrow full width at half maximum (FWHM) and high color purity, both of which are particularly important for display applications.[40] These unique emission characteristics are closely linked to precise control over the sp^2 C subdomains, which are recognized as the primary contributors to the bandgap in GQDs.[21] In this work, hydrophilic GQDs were synthesized from biomass and subsequently subjected to surface-functionalization (Scheme 1). This process not only introduced defects but also promoted aggregation, which, to the best of our knowledge, led to the first reported observation of aggregation-induced strong green fluorescence in surface-functionalized GQDs. Such modified GQDs offer multiple advantages: enhanced luminescence, the potential to induce chirality, and internal defects that serve as anchoring sites for dopant atoms. Their high biocompatibility and hydrophilic nature make them promising candidates for drug delivery, particularly in tumor and cancer-cell treatment.

© 2026 The Author(s). Published by the Royal Society of Chemistry

Furthermore, their bright luminescence and semiconducting properties render them highly attractive for luminescent-display applications.

2. Experimental

2.1   Materials

Rice husk powder (bought from Taobao, China), deionized water, NaBH$_4$, and HCl (purchased from Sinopharm Chemical Reagent, Beijing) were used in this study. For TEM study, copper grids with a holey carbon thin film were used.

2.2   Synthesis

We took *ca.* 1 g rice husk powder and dispersed it in 70 mL deionized water (DIW) in a lid-covered conical flask, and stirred for 3 hours at 1k rpm and 150 °C. The resulting solution was filtered *via* filter paper, and the formation of graphene oxide particles was confirmed *via* STEM analysis (Fig. 1a–c). The
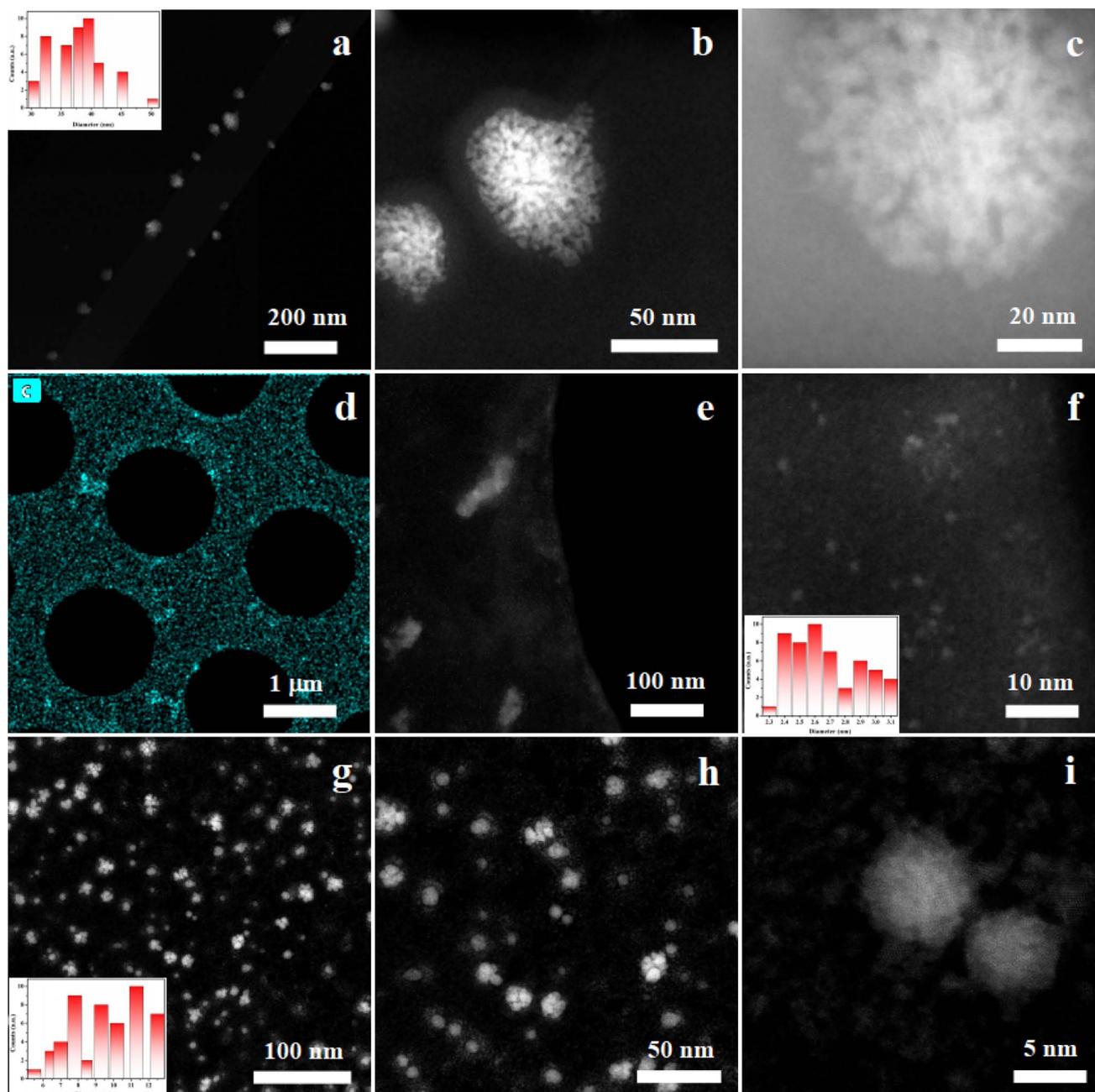

Fig. 1   Dark-field STEM images illustrating the morphological evolution of the samples: (a–c) graphene-oxide through facile synthesis from biomass after hydrothermal treatment, with scale bars of (a) 100 nm, (b) 50 nm, and (c) 20 nm; (d–f) graphene quantum dots obtained after reduction, with scale bars of (d) 1 μm, (e) 100 nm, and (f) 10 nm; (g–i) aggregated, surface functionalized-graphene quantum dots formed after acidic treatment, with scale bars of (g) 100 nm, (h) 50 nm, and (i) 5 nm.

solution was subsequently washed several times with DIW, and the obtained powder was dispersed in H_2O. An aqueous $NaBH_4$ solution was then added, and the mixture was stirred at ambient temperature for 24 h. After centrifugation at 14k rpm for 10 minutes, the supernatant was collected and characterized by UV-vis spectroscopy, FTIR, STEM, and fluorescence to confirm the presence of GQDs (Fig. 1d–f).

For surface-functionalization, the second solution was dried *via* a rotary evaporator, and the resulting powder was dissolved in HCl. The suspension was stirred continuously at 1k rpm and 50 °C for 4 h, after which HCl was removed, and the powder was washed several times with DIW. The purified sample was then redissolved in H_2O and subjected to a second reduction with an aqueous $NaBH_4$ solution under stirring for 10 hours. Finally, the sample was centrifuged under the same conditions as above, and the supernatant was analyzed by UV-vis spectroscopy, FTIR, STEM, fluorescence, photoluminescence, and XPS (Fig. 1g–i).

2.3 Instrumentation

UV-visible spectroscopy was carried out using a SHIMADZU, UV-2600i (JAPAN), and FTIR measurements were performed with a SHIMADZU, IRAffinity-1S spectrometer. HAADF images were acquired through a spherical aberration-corrected electron microscope (200 kV FEI Themis Z) at the National Graphene Products Quality Inspection and Testing Center, Wuxi, China. Fluorescence spectra were recorded with an EDINBURGH Instruments F55 spectrometer (Livingston, UK), while photoluminescence spectroscopy was conducted using a JASCO FP 6500 spectrofluorometer. X-ray photoelectron spectroscopy (XPS) measurements were performed on a Thermo Fisher Scientific K-Alpha spectrometer (England), with all spectra calibrated using the principal C 1s peak at 284.5 eV as an internal reference.

3. Results and discussion

This study provides an in-depth visualization of the morphological transformation of graphene oxide (GO) precursors into nitrogen-doped graphene quantum dots (N-GQDs), followed by their surface functionalization and aggregation under acidic treatment. Fig. 1a–c presents dark-field STEM images of GO nanosheets derived *via* a hydrothermal treatment of biomass.
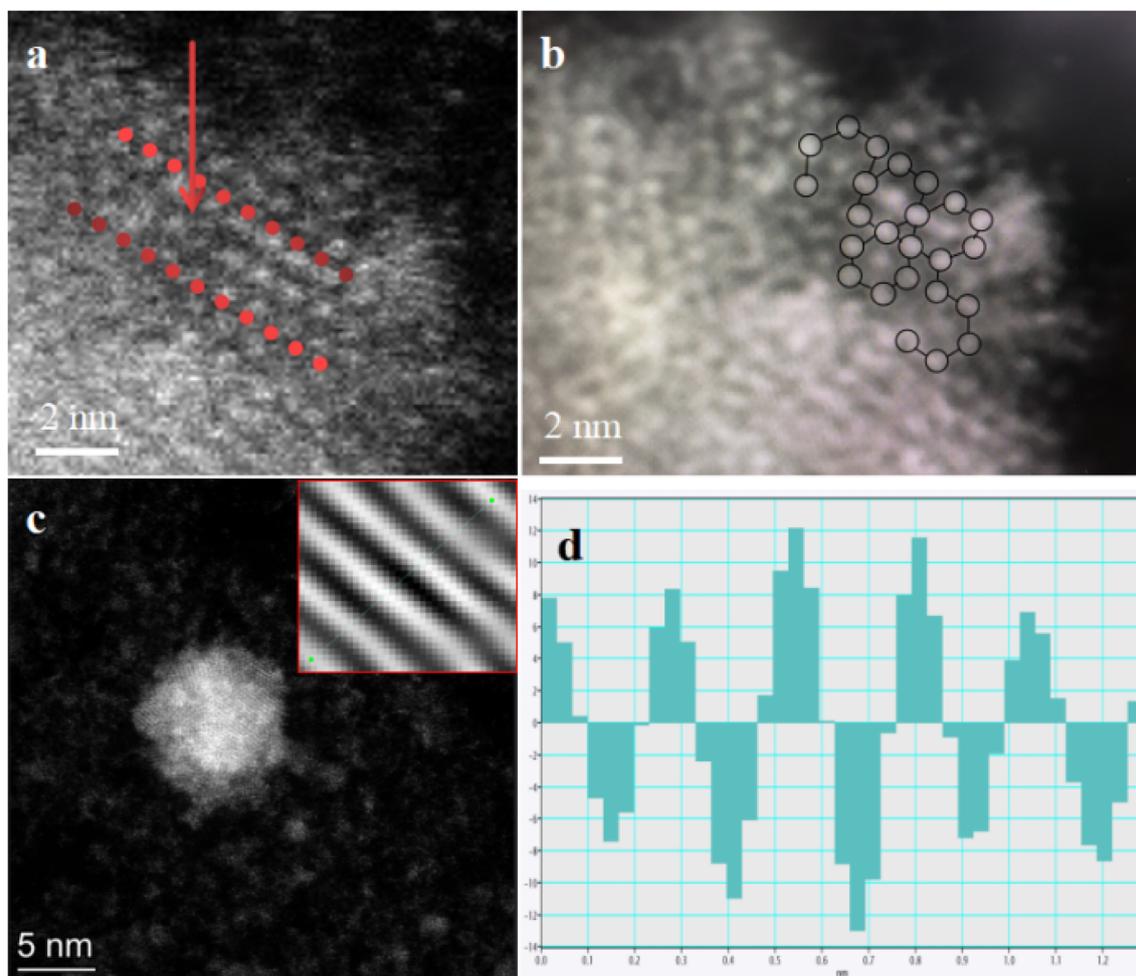

Fig. 2 Zoomed-in images of graphene quantum dots (GQDs): (a) a defect within a GQD highlighted by a dashed arrow; (b) clear visualization of atomic arrangements in {arm-chair or zigzag} configurations along with surface functionalized entities; (c and d) HRTEM image of GQDs showing lattice fringes, with interplanar spacing calculated using Digital Micrograph software.

These GO structures appear as extended, crumpled nanosheets with irregular edges and lateral dimensions exceeding 50 nm. The bright contrast and diffuse features in these images support the presence of partially oxidized carbonaceous sheets with disordered domains.[41,42] The progressive reduction in scale bars (100 nm → *ca.* 10 nm) illustrates the onset of fragmentation and edge reconstruction, which is essential for quantum dot nucleation.

Furthermore, for GQD formation, Fig. 1d–f depict the transformation from GO into GQDs after a controlled reduction step. The discrete, quasi-spherical particles observed here range in size from 3 to 10 nm, with increased brightness under dark-field conditions indicating higher electron density and compactness.[43] These GQDs are likely formed by *in situ* "cutting" of the GO sheets along defect-rich lines or oxygenated zones, a known route in biomass-derived syntheses.[44]

The final transformation stage, involving surface functionalization and aggregation, is presented in Fig. 1g and i. Acidic treatment not only induces inter-particle aggregation but also enhances luminescence. This process likely introduces carboxyl, amine, or sulfonic groups onto the GQD surface, as later confirmed by FTIR and XPS analyses. The aggregation is visually confirmed by denser clusters and overlapping boundaries, especially evident in the 5 nm resolution image (Fig. 1i), where individual dots assemble into stacked or bridged structures.[45] This clustering is hypothesized to facilitate π–π

stacking or hydrogen bonding between surface moieties, which is also correlated with the observed shift in fluorescence emission toward the green region.[41]

Fig. 2a highlights a vacancy defect, marked with a dashed arrow, showing a disruption in the otherwise periodic lattice. Such vacancy-type point defects are thermodynamically favored during oxidative cutting or post-functionalization acid treatments, particularly at higher temperatures.[46] They are key contributors to enhanced luminescence due to the formation of mid-gap states or localized energy levels.

High-resolution TEM images (Fig. 2c and d) further reveal the crystalline lattice of individual GQDs, with an interplanar spacing of approximately 0.21–0.24 nm, consistent with the (100) and (1120) planes of graphitic carbon.[47,48] This observation confirms that, despite their ultrasmall size, the dots retain high crystallinity, which is a prerequisite for their semiconducting behavior and photoluminescence efficiency.[49] Moreover, STEM images (Fig. 2) provide further insights into the structural nature of GQDs, illustrating a characteristic honeycomb structure, which is an indication of SP^2 hybridization within the carbon framework.[15,50]

GQDs commonly demonstrate an absorbance band in the UV region, spanning from 260 to 320 nm (Fig. 3a and b).[51] This absorption band originates from the π–π* transitions of sp^2 hybridized C=C bonds.[15] Occasionally, there is a less pronounced shoulder observed in the range of 270–400 nm,
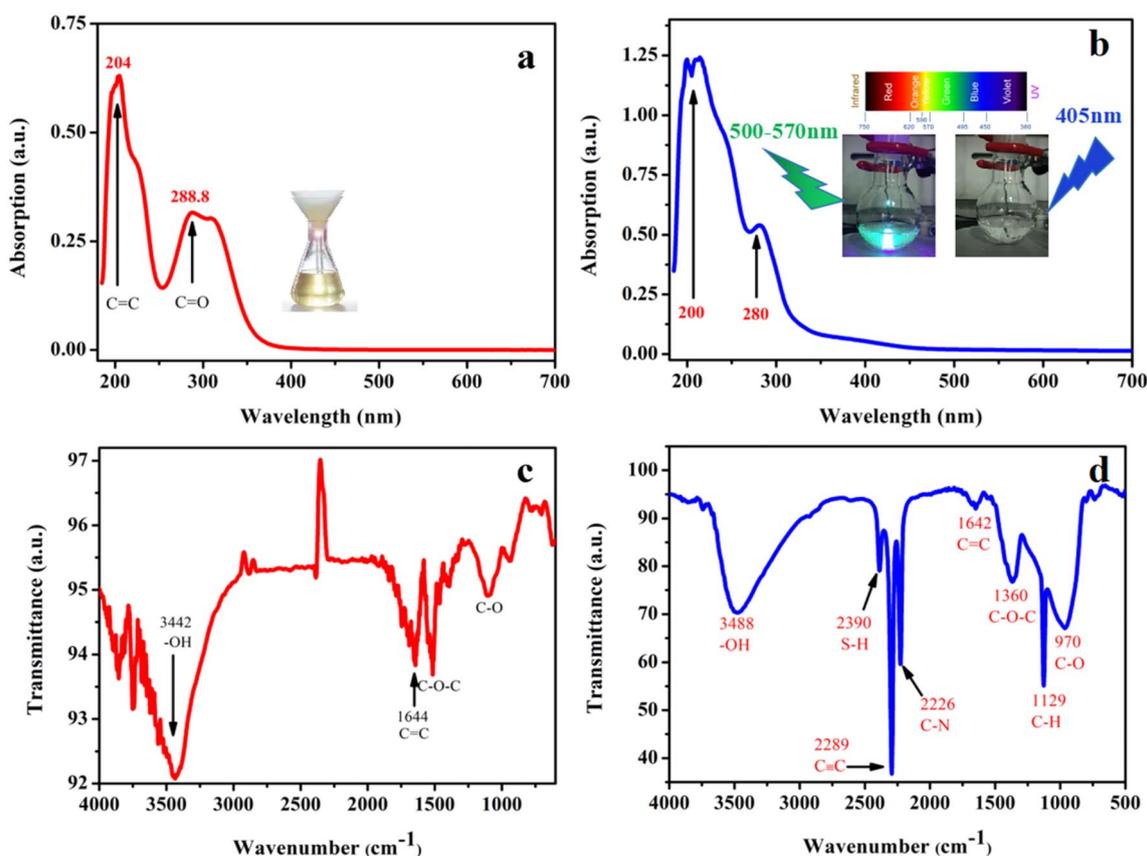

Fig. 3 (a and c) UV-vis and FTIR spectra of graphene quantum dots (GQDs) before acidic treatment, with a particle size of *ca.* 3 nm. (b and d) UV-vis and FTIR spectra of GQDs after acidic treatment, showing an increase in particle size of *ca.* 10 nm.
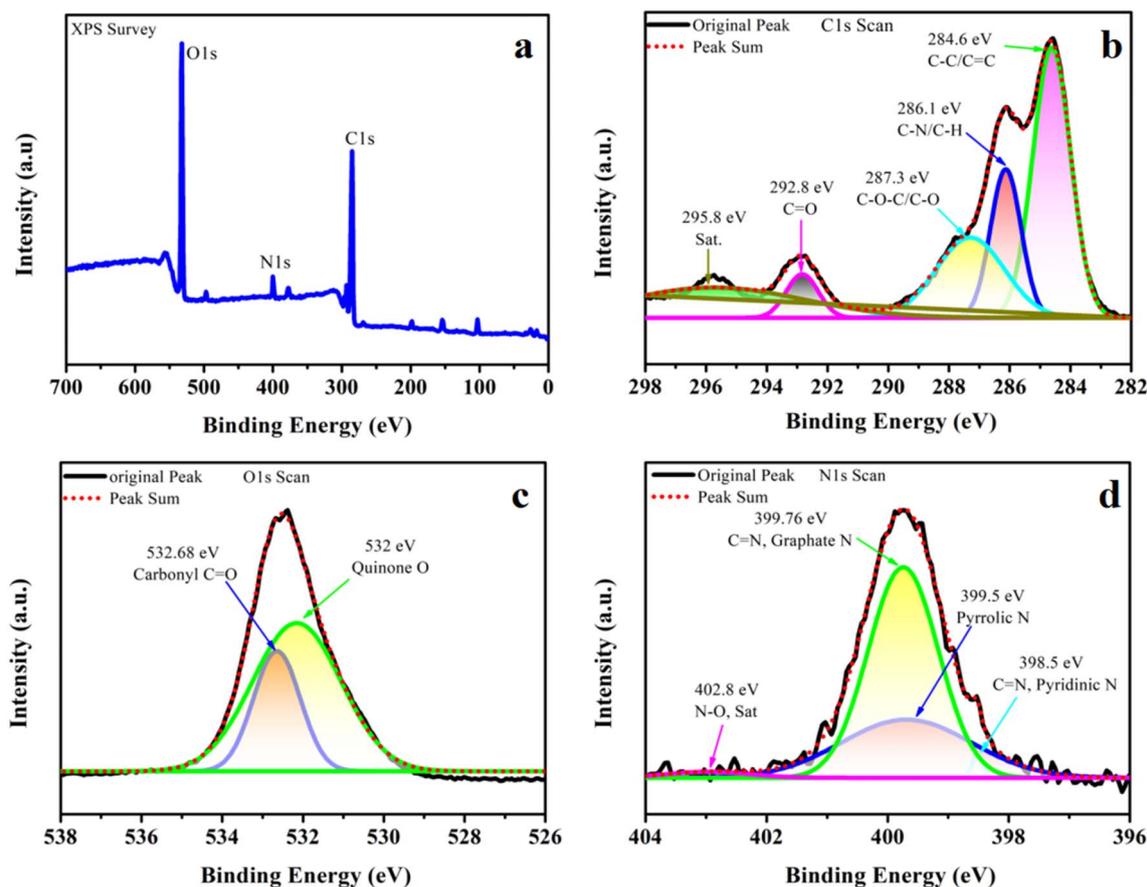
Fig. 4   XPS analysis of surface-functionalized graphene quantum dots of size *ca.* 10 nm after acidic treatment: (a) full elemental survey, (b) C 1s spectrum, (c) O 1s spectrum and (d) N 1s spectrum.

corresponding to n–π* transitions associated with carbonyl (C=O) groups, which extends into the visible wavelengths.[52] Detailed analysis of the UV-vis spectra reveals a distinct absorption peak centered at approximately 280 nm (Fig. 3b), affirming the π → π* transitions of aromatic C=C bonds.[4,53] Additionally, the presence of a shoulder beyond 300 nm reflects n → π* transitions from C=O bonds. These spectral features indicate electronic transitions within the conjugated sp^2 domains, contributing to delocalized π states that mimic the behavior observed in pristine graphene.

Interestingly, the absorption shoulder shifts from approximately 350 nm in Fig. 3a to 320 nm in Fig. 3b, which may be attributed to the HOMO to LUMO transition variations caused by surface functional groups introduced during post-synthesis treatment.[54] Complementary FTIR spectra further support these findings: the O–H stretching vibration peak at 3442 cm^{-1} in Fig. 3c became more intense and shifted to 3488 cm^{-1} in Fig. 3d, while the C=C bond stretching became more intense, confirming both sp^2 hybridization and the crystallinity of the GQDs.[55]

For small GQDs (*ca.* 3 nm), the emission peak with the highest intensity occurs at *ca.* 410 nm when excited at 320 or 310 nm (according to the trend of peak intensities) (Fig. 5a). Interestingly, the same trend has been repeated during the

excitation scan, and the peak positions are coincident (Fig. 5b). Notable shifts in peak positions, along with broadening of the full width at half maximum (FWHM), are also evident, highlighting the manifestation of the quantum confinement effect. This behaviour arises from the interplay between the surface-to-size ratio dynamics and inherent structural modifications within the GQDs.[6,21]

Similarly, for surface-functionalized GQDs, the excitation-dependent emission scan shows the highest intensity peak at 460 nm under 380 nm excitation (Fig. 5c). The same phenomenon is observed in the emission-dependent excitation scan, where the excitation peak appears at 380 nm, corresponding to emission at 460 nm (according to the trend of the peaks' intensities and positions) (Fig. 5d). The emission at 460 nm (Fig. 5c and d) originates from the n → π* transition of carbonyl or carboxylic groups associated with surface-functionalized GQDs (which are counter-confirmed by XPS (Fig. 4d)), located adjacent to the conjugated basal carbon skeleton.[56]

The broad emission arises from the layered structure of the GQDs, featuring an extensive conjugated system with widespread delocalized π electrons.[57] Consequently, the resulting GQDs exhibit wide spectral emission spanning ultraviolet to visible wavelengths (Fig. 3). This large stock shift and broad-
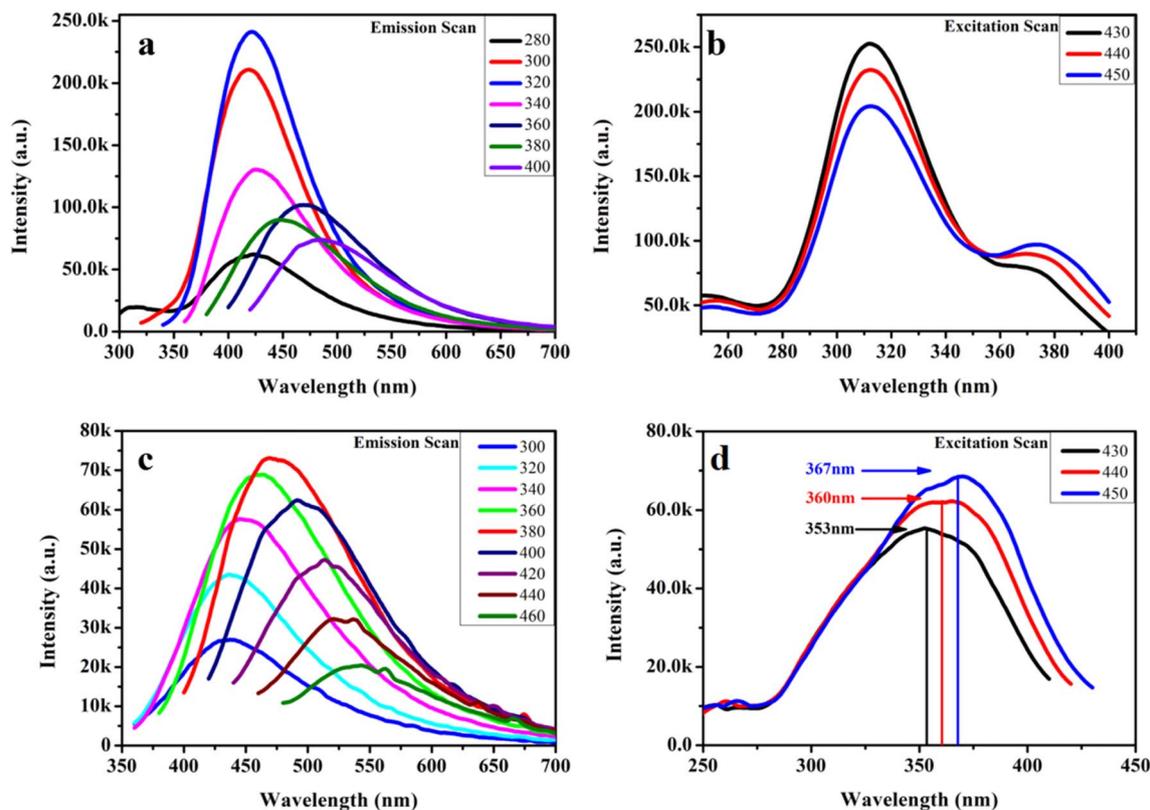
Fig. 5   Fluorescence study of GQDs: (a) emission spectrum of GQDs of size *ca.* 3 nm before acidic treatment, (b) excitation spectrum of GQDs of size *ca.* 3 nm before acidic treatment, (c) emission spectrum of surface-functionalized GQDs of size *ca.* 10 nm after acidic treatment, and (d) excitation spectrum of surface-functionalized GQDs of size *ca.* 10 nm after acidic treatment.

spectrum luminescence make them highly effective for light harvesting applications in nano-photonics, particularly in bioimaging contexts.

Typically, GQDs exhibit strong photoluminescence (PL) emissions, rendering them valuable for applications in fluorescence bioimaging.[58] The emission spectra of GQDs are intricately linked to the excitation wavelength. Variations in emission peak positions under different excitations arise from several factors such as the quantum confinement, size effects, elemental composition, edge states, surface functional groups, conjugated π-domains, and defects within the carbon framework.[59,60] These factors contribute to the existence of distinct emissive trap sites and varying electron densities on the surface of GQDs, which directly influence the PL behaviour of GQDs. Consequently, at specific excitation wavelengths, the corresponding emissive trap sites are stimulated, leading to the emission of light by GQDs (Fig. 5). These findings align harmoniously with earlier research and correlate well with the results illustrated in Fig. 3.

Moreover, depending on the solvent used, GQDs exhibit both excitation-dependent and excitation-independent fluorescence properties. The solvent-dependent fluorescence emission behavior is likely governed by solvation dynamics, further emphasizing the tunable optical properties of GQDs.[59]

The emission range of GQDs extends from 480 to 600 nm, while their excitation wavelength lies between 300 and 460 nm

(Fig. 6). GQDs exhibit excitation-dependent emission. As the excitation wavelength increases from 310 to 340 nm, the emission intensity increases (Fig. 6a). However, a further increase in excitation wavelength causes the quenching in the main peak's intensity, but another narrow emission peak appears at high energy. With continued increases in excitation wavelength, the intensity of this secondary peak not only increases, but the position of this peak also shifts to lower energy (higher wavelength) (Fig. 6b). For clarity, both excitation-dependent emissions are shown in Fig. 6c.

These spectral features result in multicolor fluorescence, with blue and green emissions being the most prominent. The quenching of blue emission at higher concentrations is attributed to aggregation-induced concentration quenching, caused by photon reabsorption and non-radiative energy transfer among aggregated GQDs. In contrast, the green emission exhibits enhanced fluorescence at high concentrations (Fig. 6c). Additionally, some studies report that GQDs exhibit up-conversion photoluminescence, also known as two-photon fluorescence, where the simultaneous absorption of two photons produces an emission wavelength shorter than the excitation wavelength (Fig. 6).

To further investigate the chemical environment and compositional changes, X-ray photoelectron spectroscopy (XPS) analysis was carried out. The entire survey XPS spectra clearly display characteristic peaks corresponding to the C 1s peak at
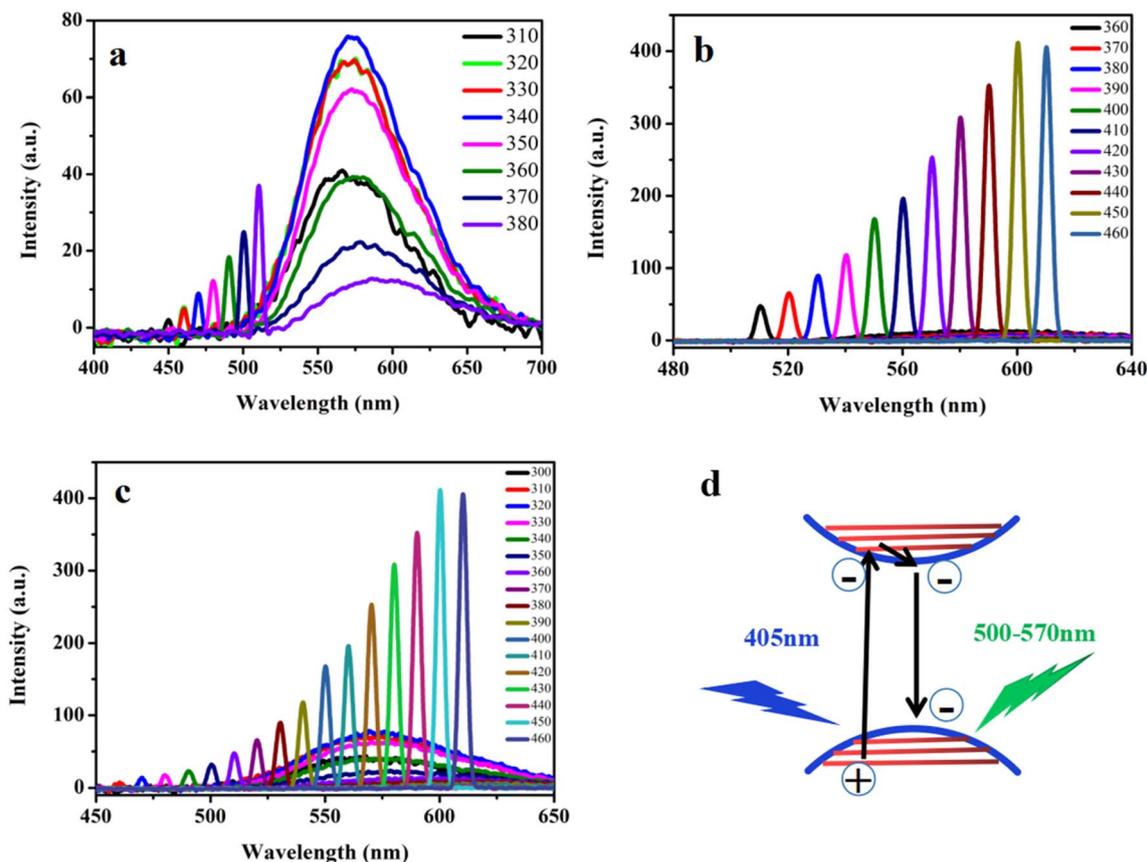
Fig. 6 Photoluminescence study of surface-functionalized graphene quantum dots of size *ca.* 10 nm after acidic treatment under different excitation energies. (a) Emission spectra of GQDs excited in the range of 310 to 380 nm. (b) Emission spectra of GQDs excited in the range of 360 nm to 460 nm. (c) Emission spectra of GQDs excited across 300 to 460 nm. (d) Schematic illustration of electron excitation and de-excitation mechanisms.

284 eV, N 1s peak at 400 eV, and O 1s peak at 532 eV (Fig. 4b). Deconvolution of the C 1s peak reveals three Gaussian peaks: the graphitic sp^2 C (C–C/C=C) is associated with the peak centered at 284.4 eV, C (C–C, C–O, and C–N) carbonyl is represented by the peaks at 285.8 eV, and the carboxylate C(O)–O is associated with the peak at 292.8 eV (Fig. 4b).[61] The N 1s peak splits into two Gaussian peaks: a small spectrum at 398.2 eV is attributed to pyrrolic N, and a dominant peak at 399.7 eV represents graphite N (Fig. 4c).[62,63]

High-resolution O 1s spectra provide further insight into oxygen functionalities. The relative contribution of carbonyl groups (C=O) increases with the pyrrolidone formation.[64]

Table 1 Comparison of biomass-derived graphene quantum dots (GQDs)

Biomass precursor	Synthesis method	Key optical properties/emission	Key advantages/novelty	Ref.
Rice husk (this work)	Hydrothermal carbonization followed by acid treatment and surface functionalization	Tunable emission; strong green fluorescence; aggregation-induced emission (AIE) for NGQDs	First report of AIE-active N-doped GQDs from rice husk	This work
Pomelo peel	Hydrothermal	Blue emission; excitation-dependent behaviour	Simple one-step synthesis from food waste	55
Waste tea	Hydrothermal	Blue-green emission	Low-cost, green synthesis from beverage waste	67
Ginger	Hydrothermal	Blue emission	Demonstrated good biocompatibility	71
Lignin	Microwave-assisted	Blue emission	High QY from lignin; rapid microwave synthesis	72
Cabbage	Hydrothermal	Blue emission	Application in photocatalysis beyond sensing	73
Rice husk (other report)	Pyrolysis & chemical oxidation	Blue emission	Rice husk-derived CDs	66

Specifically, the peak at 532.38 eV is assigned to C=O (Fig. 4d), regarded as quinone, which arises from dehydrolysis by the surrounding carboxyl groups, while the peak at 532.68 eV is associated with the carbonyl group.[65] Notably, acidic treatment not only facilitated surface functionalization and aggregation of GQDs (Fig. 5i) but also introduced inner defects within the GQDs (Fig. 6a and b). These structural modifications resulted in a notable enhancement in green fluorescence, as illustrated in the inset images of Fig. 2b.

While the synthesis of GQDs from biomass precursors like pomelo peel, tea, and ginger is well-established, these typically yield materials with common blue emission and face limitations such as aggregation-caused quenching (ACQ).[55,66,67] Our work advances this field by presenting a two-step functionalization of rice husk that produces N-doped GQDs (NGQDs) with strong, tunable green fluorescence. Crucially, and unlike the compared state of the art, our NGQDs exhibit AIE, a rare and highly valuable property that enhances their utility in solid-state applications.[68] This represents a significant departure from previous reports, including other rice husk-derived carbon dots, marking the first synthesis of AIE-active NGQDs from this abundant agricultural waste.[66] A detailed comparison of key parameters, including the precursor, synthesis route, optical properties, and novelty, is provided in Table 1, which clearly contextualizes our advancements within the recent literature. The data summarized in the table underscore that while other methods offer simplicity, our approach provides superior functional performance and a unique AIE characteristic. This combination of a scalable precursor, a controlled synthesis, and exceptional photophysical properties positions our rice husk-derived NGQDs as a superior material for advanced applications in solid-state lighting, optoelectronics, and sensing, where a high fluorescence quantum yield in aggregate states is paramount.[69,70] The table effectively highlights how our work moves beyond merely reporting another blue-emitting carbon dot to delivering a material with a distinct and practical advantage.

4. Conclusion

GQDs are a promising class of nanomaterials with immense potential, owing to their unique combination of semi-conducting behavior, size-tunable photoluminescence, and excellent biocompatibility. In this study, we report a facile, sustainable approach for the synthesis of GQDs derived from abundantly available rice husk biomass. The process involves the initial extraction of GO, its conversion into GQDs, followed by surface functionalization to yield defect-engineered GQDs exhibiting aggregation-induced green fluorescence under UV illumination. The synthesized GQDs were systematically characterized at various stages to elucidate the influence of particle size on their optical properties. Notably, the quantum confinement effect was evident, as smaller-sized GQDs demonstrated higher excitation energy requirements compared to their larger counterparts. Interestingly, upon aggregation, the smaller GQDs exhibited markedly enhanced green fluorescence under UV light, while remaining optically transparent under ambient conditions, an attribute of potential utility in stealth imaging

and optoelectronic applications. Furthermore, the excitation-dependent photoluminescence behavior of the GQDs revealed non-trivial spectral shifts, highlighting the complexity of their emissive states, possibly linked to surface defects and heterogeneity in the electronic structure. Taken together, the biomass-derived, functionally tunable GQDs reported in this study hold significant promise for applications spanning advanced opto-electronic devices and biomedical imaging platforms.

Conflicts of interest

There are no conflicts to declare.

Data availability

All data supporting the findings of this study are available within the article.

Acknowledgements

References

1 Z. Huang, Y. Shen, Y. Li, W. Zheng, Y. Xue, C. Qin, B. Zhang, J. Hao and W. Feng, *Nanoscale*, 2014, **6**(21), 13043–13052.

2 D. Pan, L. Guo, J. Zhang, C. Xi, Q. Xue, H. Huang, J. Li, Z. Zhang, W. Yu and Z. Chen, *J. Mater. Chem.*, 2012, **22**(8), 3314–3318.

3 A. Ghaffarkhah, E. Hosseini, M. Kamkar, A. A. Sehat, S. Dordanihaghighi, A. Allahbakhsh, C. van der Kuur and M. Arjmand, *Small*, 2022, **18**(2), 2102683.

4 X.-J. Jin, L. Tan, Z.-Q. Zhao, M.-C. Li, Q.-Y. Zhou, J.-J. Zhang, T.-B. Lv, Q. Deng, J. Wang and Z. Zeng, *New J. Chem.*, 2023, **47**(5), 2221–2229.

5 M. Zhang, L. Bai, W. Shang, W. Xie, H. Ma, Y. Fu, D. Fang, H. Sun, L. Fan and M. Han, *J. Mater. Chem.*, 2012, **22**(15), 7461–7467.

6 S. A. Shah, K.-J. Hu, M. Naveed, C. Lu and S. Hu, *Chem. Phys. Lett.*, 2023, **811**, 140206.

7 S. K. Lai, C. M. Luk, L. Tang, K. S. Teng and S. P. Lau, *Nanoscale*, 2015, **7**(12), 5338–5343.

8 S. A. Shah, A. H. Pato, S. Jangra, A. A. Mahmud, I. H. Sajid, P. Rosaiah, K. Singh, H. Bandi, M. Z. Khan, M. Shkir, S. Rizwan, T. L. Tamang and I. Hussain, *Nano Res.*, 2025, **18**(9), 94907855.

9 F. Fei, S. Zhang, M. Zhang, S. A. Shah, F. Song, X. Wang and B. Wang, *Adv. Mater.*, 2020, **32**(27), 1904593.

10 E. Gul, S. A. Shah and S. N. A. Shah, *Biomass-Based Supercapacitors: Design, Fabrication and Sustainability*, 2023, pp. 179–200.

11 P. Ezati, R. Priyadarshi and J.-W. Rhim, *Sustainable Mater. Technol.*, 2022, e00494.

12 H. Sun, L. Wu, N. Gao, J. Ren and X. Qu, *ACS Appl. Mater. Interfaces*, 2013, **5**(3), 1174–1179.

13 V. Georgakilas, J. A. Perman, J. Tucek and R. Zboril, *Chem. Rev.*, 2015, **115**(11), 4744–4822.

14 H. Sun, L. Wu, W. Wei and X. Qu, *Mater. Today*, 2013, **16**(11), 433–442.

15 B. Park, S. J. Kim, J. S. Sohn, M. S. Nam, S. Kang and S. C. Jun, *Nano Res.*, 2016, **9**, 1866–1875.

16 P. Kaur and G. Verma, *Mater. Today Sustain.*, 2022, **18**, 100137.

17 N. V. Tepliakov, E. V. Kundelev, P. D. Khavlyuk, Y. Xiong, M. Y. Leonov, W. Zhu, A. V. Baranov, A. V. Fedorov, A. L. Rogach and I. D. Rukhlenko, *ACS Nano*, 2019, **13**(9), 10737–10744.

18 X. Yao, R. E. Lewis and C. L. Haynes, *Acc. Chem. Res.*, 2022, **55**(23), 3312–3321.

19 N. Sohal, B. Maity and S. Basu, *RSC Adv.*, 2021, **11**(41), 25586–25615.

20 M. J. Im, J. I. Kim, S. K. Hyeong, B. J. Moon and S. Bae, *Small*, 2023, **19**(47), 2304497.

21 H. Cho, G. Bae and B. H. Hong, *Nanoscale*, 2024, **16**(7), 3347–3378.

22 S. Wang, I. S. Cole, D. Zhao and Q. Li, *Nanoscale*, 2016, **8**(14), 7449–7458.

23 T. Du, J. She, X. Yang, Y. Zhao, S. Zhou and J. Zhao, *Appl. Phys. Lett.*, 2023, **122**(14), 142107.

24 Z. Qian, J. Ma, X. Shan, L. Shao, J. Zhou, J. Chen and H. Feng, *RSC Adv.*, 2013, **3**(34), 14571–14579.

25 S. H. Jin, D. H. Kim, G. H. Jun, S. H. Hong and S. Jeon, *ACS Nano*, 2013, **7**(2), 1239–1245.

26 J. Wang, H.-b. Sun, S. A. Shah, C. Liu, G.-y. Zhang, Z. Li, Q.-f. Zhang and M. Han, *Int. J. Hydrogen Energy*, 2020, **45**(19), 11089–11096.

27 T. Henna and K. Pramod, *Mater. Sci. Eng. C*, 2020, **110**, 110651.

28 Y. Li, H. Shu, S. Wang and J. Wang, *J. Phys. Chem. C*, 2015, **119**(9), 4983–4989.

29 S. Kim, S. W. Hwang, M.-K. Kim, D. Y. Shin, D. H. Shin, C. O. Kim, S. B. Yang, J. H. Park, E. Hwang and S.-H. Choi, *ACS Nano*, 2012, **6**(9), 8203–8208.

30 H. Abdelsalam, H. Elhaes and M. A. Ibrahim, *Chem. Phys. Lett.*, 2018, **695**, 138–148.

31 J. Feng, Q. Guo, H. Liu, D. Chen, Z. Tian, F. Xia, S. Ma, L. Yu and L. Dong, *Carbon*, 2019, **155**, 491–498.

32 S. Chen, N. Ullah, T. Wang and R. Zhang, *J. Mater. Chem. C*, 2018, **6**(25), 6875–6883.

33 J. Zhang, Z. Zhao, Z. Xia and L. Dai, *Nat. Nanotechnol.*, 2015, **10**(5), 444–452.

34 D. Yu, Y. Xue and L. Dai, *J. Phys. Chem. Lett.*, 2012, **3**(19), 2863–2870.

35 T. F. Yeh, C. Y. Teng, S. J. Chen and H. Teng, *Adv. Mater.*, 2014, **26**(20), 3297–3303.

36 N. Ranjbar Sahraie, J. P. Paraknowitsch, C. Göbel, A. Thomas and P. Strasser, *J. Am. Chem. Soc.*, 2014, **136**(41), 14486–14497.

37 Q. Liu, B. Guo, Z. Rao, B. Zhang and J. R. Gong, *Nano Lett.*, 2013, **13**(6), 2436–2441.

38 Y. Qu, F. He, C. Yu, X. Liang, D. Liang, L. Ma, Q. Zhang, J. Lv and J. Wu, *Mater. Sci. Eng. C*, 2018, **90**, 764–780.

39 L. Feng, L. Wu and X. Qu, *Adv. Mater.*, 2013, **25**(2), 168–186.

40 H. Yoon, H. S. Kim, J. Kim, M. Park, B. Kim, S. Lee, K. Kang, S. Yoo and S. Jeon, *ACS Appl. Nano Mater.*, 2020, **3**(7), 6469–6477.

41 Y. Wang, Y. Liu, H. Zhang, X. Duan, J. Ma, H. Sun, W. Tian and S. Wang, *Chem. Soc. Rev.*, 2025, **54**(5), 2436–2482.

42 J.-P. Da Costa, P. Weisbecker, B. Farbos, J.-M. Leyssale, G. Vignoles and C. Germain, *Carbon*, 2015, **84**, 160–173.

43 S. Liu, Y. Xu, X. Wang, H. Zhou and T. Zhang, *Chem. Eng. J.*, 2024, **496**, 153914.

44 B. Zhang, Y. Jiang and R. Balasubramanian, *J. Mater. Chem. A*, 2021, **9**(44), 24759–24802.

45 Y. Ru, G. I. Waterhouse and S. Lu, *Aggregate*, 2022, **3**(6), e296.

46 K. K. Chan, S. H. K. Yap and K.-T. Yong, *Nano-Micro Lett.*, 2018, **10**, 1–46.

47 M. Ali, R. Riaz, A. S. Anjum, K. C. Sun, H. Li, S. H. Jeong and M. J. Ko, *Carbon*, 2021, **171**, 493–506.

48 R. Das, H. Sugimoto, M. Fujii and P. Giri, *ACS Appl. Mater. Interfaces*, 2020, **12**(4), 4755–4768.

49 X. T. Tian and X. B. Yin, *Small*, 2019, **15**(48), 1901803.

50 P. Tian, L. Tang, K. Teng and S. Lau, *Mater. Today Chem.*, 2018, **10**, 221–258.

51 A. Bokare, D. Nordlund, C. Melendrez, R. Robinson, O. Keles, A. Wolcott and F. Erogbogbo, *Diamond Relat. Mater.*, 2020, **110**, 108101.

52 T. Gao, X. Wang, L.-Y. Yang, H. He, X.-X. Ba, J. Zhao, F.-L. Jiang and Y. Liu, *ACS Appl. Mater. Interfaces*, 2017, **9**(29), 24846–24856.

53 Z.-Q. Zhao, L. Tan, T.-B. Lv, J.-J. Zhang, K.-M. Liao, H.-Y. Wang, Z. Zeng, S. Deng and G.-P. Dai, *ACS Appl. Nano Mater.*, 2024, **7**(11), 13736–13744.

54 J. Peng, J. Gao, B. K. Gupta, Z. Liu, R. Romero-Aburto, L. Ge, L. Song, L. B. Alemany, X. Zhan and G. Gao, *Nano Lett.*, 2012, **12**(2), 844–849.

55 S. Zhu, Q. Meng, L. Wang, J. Zhang, Y. Song, H. Jin, K. Zhang, H. Sun, H. Wang and B. Yang, *Angew. Chem., Int. Ed.*, 2013, **52**(14), 3953–3957.

56 Z. Li, Z. Liu, H. Sun and C. Gao, *Chem. Rev.*, 2015, **115**(15), 7046–7117.

57 A. Xu, G. Wang, Y. Li, H. Dong, S. Yang, P. He and G. Ding, *Small*, 2020, **16**(48), 2004621.

58 Y. Dai, H. Long, X. Wang, Y. Wang, Q. Gu, W. Jiang, Y. Wang, C. Li, T. H. Zeng and Y. Sun, *Part. Part. Syst. Charact.*, 2014, **31**(5), 509.

59 R. V. Nair, R. T. Thomas, V. Sankar, H. Muhammad, M. Dong and S. Pillai, *ACS Omega*, 2017, **2**(11), 8051–8061.

60 S. A. Shah, K.-J. Hu, M. Naveed, S. N. A. Shah, S. Hu, S. Lu and F. Song, *Mater. Res. Express*, 2019, **7**(1), 016506.

61 D. Wei, Y. Liu, Y. Wang, H. Zhang, L. Huang and G. Yu, *Nano Lett.*, 2009, **9**(5), 1752–1758.

62 Y. Fang, S. Guo, D. Li, C. Zhu, W. Ren, S. Dong and E. Wang, *ACS Nano*, 2012, **6**(1), 400–409.

63 W. Ding, Z. Wei, S. Chen, X. Qi, T. Yang, J. Hu, D. Wang, L. J. Wan, S. F. Alvi and L. Li, *Angew. Chem.*, 2013, **125**(45), 11971–11975.

64 S. Chen, X. Hai, C. Xia, X. W. Chen and J. H. Wang, *Chem.– Eur. J.*, 2013, **19**(47), 15918–15923.

65 Z. L. Wu, P. Zhang, M. X. Gao, C. F. Liu, W. Wang, F. Leng and C. Z. Huang, *J. Mater. Chem. B*, 2013, **1**(22), 2868–2873.

66 V. Wongso, N. S. Sambudi, S. Sufian and Isnaeni, *Biomass Convers. Biorefin.*, 2021, **11**(6), 2641–2654.

67 A. Prasannan and T. Imae, *Ind. Eng. Chem. Res.*, 2013, **52**(44), 15673–15678.

68 T. J. Pillar-Little Jr, Carbon Quantum Dots: Bridging the gap between chemical structure and material properties, PhD thesis, 2017, DOI: **10.13023/ETD.2018.108**.

69 N. Xie, L. Tan, H.-F. Li, H.-Y. Hu, C. Wang, M. Pan, F. Wu, P. Wu, X.-D. Wang and Z. Zeng, *J. Lumin.*, 2020, **219**, 116827.

70 Z. Liu, L. Tan, P.-P. Hou, X.-J. Jin, M.-C. Li, Q.-Y. Zhou, P. Liao, Z. Zeng, S. Deng and G.-P. Dai, *Opt. Mater.*, 2022, **127**, 112368.

71 W. Liu, H. Diao, H. Chang, H. Wang, T. Li and W. Wei, *Sens. Actuators, B*, 2017, **241**, 190–198.

72 X. Xu, X. Wang, W. Du, S. Liu, Z. Qiao and Y. Zhou, *Nanotechnol. Rev.*, 2025, **14**(1), 20250184.

73 A. S. Sharma, S. Ali, D. Sabarinathan, M. Murugavelu, H. Li and Q. Chen, *Compr. Rev. Food Sci. Food Saf.*, 2021, **20**(6), 5765–5801.